Lysozyme conformational changes with ionic liquids: spectroscopic, small angle x-ray scattering and crystallographic study

Qi Han[1], Kate M. Smith[2], Connie Darmanin[3], Timothy M. Ryan[2], Calum J. Drummond[1], Tamar L. Greaves[1]*

[1]School of Science, College of Science, Engineering and Health, RMIT University, 124 La Trobe Street, Melbourne, VIC 3000, Australia. [2] Australian Synchrotron, Australian Nuclear Science and Technology Organisation, 800 Blackburn Road, Clayton, VIC, 3168, Australia. [3] ARC Centre of Excellence in Advanced Molecular Imaging, Department of Chemistry and Physics, La Trobe Institute for Molecular Sciences, La Trobe University, VIC 3086, Australia. *E-mail: tamar.greaves@rmit.edu.au

Abstract

Solvents that support protein functionality are important for biochemical applications, and new solvents are required. Here we employ FTIR and fluorescence spectroscopies, small angle X-ray scattering (SAXS) and X-ray crystallography to understand conformational changes of lysozyme with ionic liquids (ILs) added. Spectroscopic techniques identified that the secondary structure of lysozyme was maintained at the lower IL concentrations of 1 and 5 mol%, though the Tryptophan environment was significantly altered with nitrate-based ILs present. SAXS experiments indicated that the radius of gyration of lysozyme increased with 1 mol% IL present, and then decreased with increasing IL concentrations. The tertiary structure, particularly the loop regions, changed as a function of IL concentration, and this depended on the IL type. The crystallographic structure of lysozyme with the IL of ethylammonium nitrate present confirmed the loop region was extended, and identified three specific binding sites with nitrate ions, and that the positively charged areas were IL sensitive regions. This work provides a detailed understanding of lysozyme conformational changes in the presence of ILs. This approach can be extended to other functionally-important proteins.

Keywords: ionic liquid, lysozyme, protein stability, FTIR, fluorescence, small-angle X-ray scattering (SAXS), crystallography, conformational change

1. Introduction

Proteins are abundant and complex macromolecules that are found in all cells, and are important for biological functions. The amino acid sequence, and their interactions, determine the particular structure of proteins, and this generally dominates their biological functions. Understanding protein structure-function relationships is a key requirement for advancing technological development in the biotechnology industry, pharmacology, and in fundamental molecular biology studies. The unique conformations of proteins can be easily altered by, for example, denaturants such as heat, acid, alkali, concentrated urea, organic solvents, and detergents[1]. Consequently, external factors have been extensively studied in protein chemistry for controlling protein behavior, such as solubility, stability, activity (for enzymes) and crystallization[1-2].

Water is the universal and natural solvent for proteins. However, it cannot satisfy the solvent requirements for many desirable protein applications. Hence numerous studies have pursued alternative solvents to identify those which can improve protein stability[2-3]. Traditional molecular organic solvents have been trialed, though they often lead to insufficient protein stability, and are typically volatile[4]. As an alternative solvent class to volatile media (i.e., water and organic solvents), ionic liquids (ILs) with low and negligible-volatility have drawn a lot of attention in recent decades as potential solvents for biological molecules[5-6]. ILs are liquids that are comprised of ions and have highly tunable properties through modification of the cation and anion structures[7-9]. Protic ILs (PILs) are a subclass of ILs which are formed through proton transfer from a Brønsted acid to a Brønsted base. This results in a hydrogen that is available for hydrogen bonding, which is a key feature of PILs[8, 10]. Most proteins generally suffer from low activity, stability and selectivity in neat ILs, and in recent years research efforts have been devoted to developing more compatible and improved IL systems for protein stabilization and biocatalysis[5-6]. In particular, the use of IL mixtures, especially with water, has achieved a range of desirable solvent properties for proteins[5, 11-12]. For example, aqueous PIL solutions of ethylammonium nitrate (over 10 mol% PIL) have been used to improve the solubility and stability of cytochrome *c*[13] and lysozyme[14]. However, the lysozyme was shown to be unfolded in high concentration of ILs [14-16].

The ideal 1:1 stoichiometry of the cation:anion for PILs is difficult to achieve in practice, and small variations can substantially change the pH of IL-water mixtures[9]. Previously, we have reported that non-stoichiometric PIL-water mixtures can be used for stabilization of lysozyme and lipase, which indicates some tolerance towards changes in pH due to non-stoichiometry[17-

[18]. In addition, pH-stable IL systems have been developed for biocatalysis through the addition of small proportions of buffering agents[19]. In terms of IL selection, many previous studies have shown that the anion can dominate the IL properties[20]. For example, mesylate based ILs[12, 18] and choline coupled with dihydrogen phosphate (DHP)[21] have been reported as bio-compatible ILs for proteins. However, we have also reported in a previous study on aqueous PILs containing nitrate or carboxylate anions that the cation, and cation-anion combination, can have a strong influence, where ethylammonium nitrate (EAN) and ethanolammonium formate (EtAF) stabilized lysozyme, whereas ethylammonium formate (EAF) and ethanolammonium nitrate (EtAN) were poor solvents for lysozyme[17, 22]. However, the preference of the ions can be related to the specific ion effect of proteins in the solution, which is due to the effect of ions on the local water structure and hydration of proteins[11].

The protein structural stability in the solvent is controlled by the inter and intra interactions between the protein molecules and the solvent species[2]. The interaction of ILs with proteins include ionic, hydrogen-bond and polar interactions. It is generally acknowledged that functionally important amino acid residues are mainly solvent-accessible on the protein surface, while structurally important residues are part of the protein core[2]. A range of techniques have been utilized to understand protein structure and interactions. The amide I band (1700−1600 cm^{-1} region) is the most sensitive spectral region to the protein secondary structure for infrared spectroscopy and is due to the C=O stretching modes of the peptide linkages[23]. NMR techniques are time-consuming, while growing crystals for protein crystallography can be challenging. Therefore, these techniques are not suitable for high-throughput IL screening, which is needed to identify ILs with prospective properties. Instead, solution-based techniques, such as spectroscopic methods and small angle X-ray scattering (SAXS), have been used to explore the structure of proteins in a broad range of IL systems[17]. In recent years, the quality and throughput of SAXS experimental data has improved dramatically, and there has been an increase in the accuracy and quality of SAXS profiles[24].

Very limited work has been focused on understanding complex protein-IL solvent interactions, with the exception of recent studies using NMR[25-26] and crystallography[27]. These studies have shown the specific interaction of the anions of ILs with proteins. However, detailed protein structural analysis can be achieved from SAXS data, though requires accurate and sufficiently precise SAXS patterns (systems with the subtracted solvent contribution, and free of nonspecific aggregation or interparticle interference). SAXS can be used to characterize unique

aspects of the protein shape[28]. In addition, ab initio bead modelling and/or atomistic modelling using domains of known structure (derived from crystallography or NMR experiments) can be used to get greater information from SAXS about the protein shape[29].

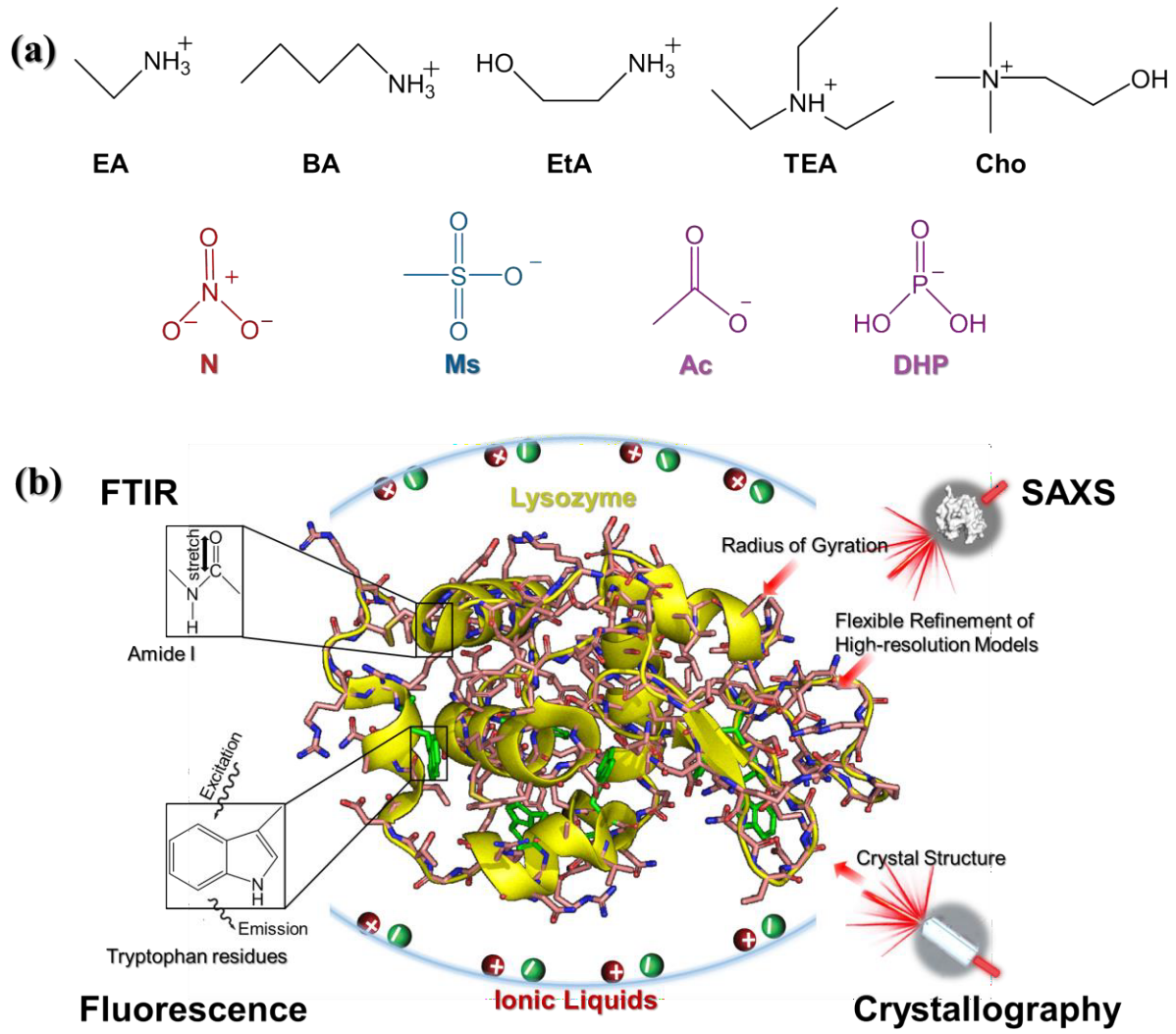

Figure 1. (a) Structures of the cations (ethylammonium (EA), butylammonium (BA), ethanolammonium (EtA), triethylammonium (TEA), and choline (Cho)) and anions (nitrate (N), mesylate (Ms), acetate (Ac) and dihydrogen phosphate (DHP)) with their abbreviations used in this work. (b) Schematic of the four techniques used for investigating conformational changes of lysozyme in ionic liquid-water mixtures.

In this study, hen egg white lysozyme was used as a model protein, as it is a well-folded globular protein with ~40% α-helix and 10% β-sheet structures (6% antiparallel β-sheet) and considered as a near-spherical object [23, 30]. Nine ILs were selected to enable structure-property relationships

to be developed, using the ions in Figure 1a. These were ethylammonium nitrate (EAN), butylammonium nitrate (BAN), ethanolammonium nitrate (EtAN), ethylammonium mesylate (EAMs), triethylammonium mesylate (TEAMs), choline mesylate (ChoMs), choline acetate (ChoAc), triethylammonium dihydrogen phosphate (TEADHP) and choline dihydrogen phosphate (ChoDHP). Two PIL concentrations in water of 1 and 5 mol% were the focus of the current study, with 10 and 16.7 (ca. 17) mol% used for comparison, since they include dilute, intermediate, concentrated and hydrated PILs. The pH was maintained at 8 for most solutions. Spectroscopic and SAXS techniques were employed to gain insight into the conformational changes of lysozyme in IL-water mixtures. Furthermore, we were able to crystallize the lysozyme in an EAN-water mixture, and the crystal model was included for conformational analysis. A summary of the techniques is provided in Figure 1b. The structural analysis is discussed in detail and used for an in-depth investigation of the structure of lysozyme in these IL systems.

2. Materials and Methods

2.1. Sample preparation

Ethylamine (70% in methanol), n-Butylamine (99.5%), ethanolamine (99%), triethylamine (≥99%), choline hydroxide (45% in methanol), nitric acid (70%), glacial acetic acid (>99.8%), methanesulfonic acid (>99.5%), phosphoric acid (≥85% in water) were obtained commercially from Sigma Aldrich and were all used without further purification. Choline dihydrogen phosphate (>98%) was purchased from Io-Li-Tec, Germany. The other ILs were synthesized as reported previously[21, 31-32]. In brief, the ILs were synthesized by neutralizing equimolar amounts of the corresponding acid and base. Excess water was removed under reduced pressure using a rotary evaporator followed by a freeze dryer. The water content of the ILs (solid ILs were dissolved in methanol) was measured using a Karl Fisher coulometer (Mettler Toledo DL39). The water content of all ILs was below 0.5 wt% after drying. The purity of ILs was confirmed by NMR. For the aqueous ILs, a specified amount of the ILs were gravimetrically mixed with MilliQ water to reach the required concentration (Table S1, ESI). The pH of the aqueous IL solutions was measured using a pH meter (Mettler Toledo) and then adjusted to an apparent pH of 8 by titrating with 2 M tris(hydroxymethyl)aminomethane (Tris) as previously described[19]. The molar concentration of the ions had very little change by the buffering. Taking 1 mol% and 16.66 mol% as examples, the concentration of total ions increased to 1.003 and 16.737 mol% after buffer addition, respectively.

Lysozyme from chicken egg white powder (E.C. 3.2.1.17; product code L6878) was obtained commercially from Sigma Aldrich and used as received. Lysozyme stock solutions were prepared by dissolving 200 mg/mL lysozyme lyophilized powder in Tris buffer (100 mM, pH 8 or acetate buffer (0.1 M, pH 4). By mixing with IL-water mixtures, the protein concentration was adjusted to 20 mg/mL for FTIR and 5 mg/mL for fluorescence and SAXS experiments, respectively.

2.2. Characterizations

FTIR experiments were conducted using a Perkin Elmer spectrum 100/Universal diamond attenuated total reflectance (FTIR/ATR). Lysozyme (20 mg/mL) was equilibrated in each solvent for 1 hour before measurement. Each spectrum consisted of 64 scans with a resolution of 4 cm^{-1}. The amide I band region (1550 – 1750 cm^{-1}) was selected for analysis. Careful

background subtraction with each solvent was performed to minimize solvent contributions[33]. The spectra were smoothed (Savitzky-Golay) and normalized to the same intensity for ease of spectral comparison.

The fluorescence spectra were collected using a Perkin Elmer EnSight Multimode Plate Reader. Protein samples were equilibrated for 1 hour before measurement. The fluorescence emission was recorded from 305 to 450 nm, with excitation at 290 nm. The spectra were plotted, a smoothing algorithm (Savitzky-Golay) applied, and the relative fluorescence calculated from the fluorescence of the protein in the IL sample relative to that of the protein in the buffer.

SAXS experiments were carried out at the SAXS/WAXS beamline at the Australian Synchrotron, Melbourne, Australia. The setup had an automated well plate system, where each sample and the blank solvent was drawn into the same capillary to enable accurate buffer subtraction, as reported in our previous work[17, 33]. Ten successive frames of 1 s exposure were collected for each sample under flow. This system has been designed for weakly-scattering protein samples and reduces protein damage through minimizing the X-ray radiation dose per molecule. Lysozyme samples were equilibrated for 1 hour before measurement, and 50 µL of each sample was loaded into the 96-well plate used for the automated sampling setup. The q-range for all the SAXS experiments was 0.006 to 0.53 $Å^{-1}$. Details of data collection can be found in Table S2 of the ESI.

Scatterbrain 2.82 was used for SAXS data processing, and Chromixs and SREFLEX of the ATSAS software package were used for SAXS data analysis[34-35]. SAXS patterns are presented as the average of the measurements after careful blank subtraction of the corresponding solvent[36]. The patterns are presented offset for comparison in the figures. The radius of gyration (R_g) for lysozyme was calculated from the Guinier approximation through the ATSAS package. The distance distribution function P(r) and the maximum diameter (D_{max}) were also obtained using the ATSAS software. CRYSOL was used to screen different lysozyme crystal structures (PDB ID 1dpw, 1dpx, 1lkr, 1lks, 1uco, 3a8z, 3ru5, 3wul, 3wum, 3wun and 193l), and 1dpw was selected as the closest match to the SAXS patterns. The crystallization buffer for 1dpw contained 50 mM Tris pH 8.0 and 70%(v/v) 2-methyl-2,4-pentanediol at pH 8[37]. SREFLEX was used for refinement and normal mode analysis from the initial structure (1dpw)[34]. The discrepancies χ^2 values of the initial structure with the SAXS patterns were provided, while the best refined models in different ILs were selected based on the χ^2 values. An open-source

PyMOL v. 1.8.4.0 (https://pymol.org/) was used to visually analyze and generate figures. The surface electrostatic representation was prepared using APBS (Adaptive Poisson-Boltzmann Solver) [38].

For the crystallography experiment, lysozyme was crystallized using the batch method. A stock solution of 200 mg/mL lysozyme in Tris buffer, pH 8, was prepared and diluted 10-fold in 1 mol% EAN-water mixture (pH 8), resulting in a final concentration of 20 mg/mL. The sample was left to precipitate and crystallize overnight. A routine crystallography experiment was carried out where 1 crystal was isolated from the crystal solution and transferred to a cryo-protectant (Paratone® 8277, Hampton Research). The crystal was immediately flash-frozen in liquid nitrogen and mounted on the MX2 macromolecular beamline at the Australian Synchrotron. Data collection was carried out at 100 K on a single crystal. X-ray diffraction patterns were collected on the MX2 beamline using the Australian Cancer Research Foundation Dectris Eiger 16 M detector[39]. Data reduction and integration were performed using XDS[40]. Merging, indexing and scaling was done using Aimless and the CCP4 suite[41], and 5% of the reflections were used for the R_{free} calculations. Phaser was used to phase the model using the molecular replacement approach with 1dpw used as the search model[42]. Iterative cycles of model building and refinement were performed with Coot[43] and Phenix v1.8[44], respectively. Data collection and refinement statistics can be found in Table S3.

3. Results and discussion

3.1. FTIR and fluorescence spectroscopic study of lysozyme

FTIR spectra of lysozyme in the IL-water mixtures were investigated, and changes in the amide I band (1650 cm^{-1}) of lysozyme are shown in Figure 2 with respect to the control sample, i.e., lysozyme in buffer (Tris pH 8 or pH 4). In order to consider the total ion concentration in the IL-water mixtures, and to compare the effect of the different ions, we have represented the IL concentration in mol%. Lysozyme in EAN-water solutions containing 1 to 100 mol% EAN were initially explored. Concentrations of 1 and 5 mol% of the other PILs in water were then selected for study, based on the EAN results, and on previous studies[17, 22]. Additional higher concentrations were included for some PILs, e.g., 10 mol% for most ILs, and 17 mol% for hydrated TeaDHP and ChoDHP. It should be noted that the pH of the TEADHP and ChoDHP IL solutions were approximately 4, with a pH 4 buffer used for comparison for these.

Figure 2a shows the amide I band (1700-1600 cm^{-1} region) of lysozyme in EAN-water mixtures as a function of IL concentration. The spectra of lysozyme in EAN 1 mol% and 5 mol% had a peak at ~ 1650 cm^{-1}, and had a similar shape as lysozyme in buffer (pH 8), suggesting that the α-helix structure is well-maintained[30]. However, in higher concentrations of EAN (e.g. 10, 17, 33, and 100 mol% EAN), the peak of the amide I band was redshifted, and the band was inhomogeneously broadened. In particular, an additional peak developed around 1609 cm^{-1}, and the main peak shifted to ~1662 cm^{-1} in both 33 and 100 mol% EAN, which is indicative of intermolecular antiparallel β-sheet aggregation[30, 45]. The β-sheet shoulder, which would be observed at the high-frequency edge (1680 cm^{-1}) of the amide I band, is not distinct for native lysozyme since it has only 6.2% β-sheet. This shift is attributed to unfolding in the helical structure and aggregate formation upon removal of water molecules at high concentrations of EAN, consistent with previous publications[30, 33, 45]. It is likely that the α-helix and β-sheets changed to loops[17, 46], though it is difficult to correlate the spectral profiles observed in the amide I peak with specific lysozyme structural elements. Based on the results for EAN, two IL concentrations of 1 and 5 mol% were the focus in the following studies to observe the smaller structural changes where lysozyme is nominally stable, along with 10 mol% of the ILs where some larger structural changes were likely.

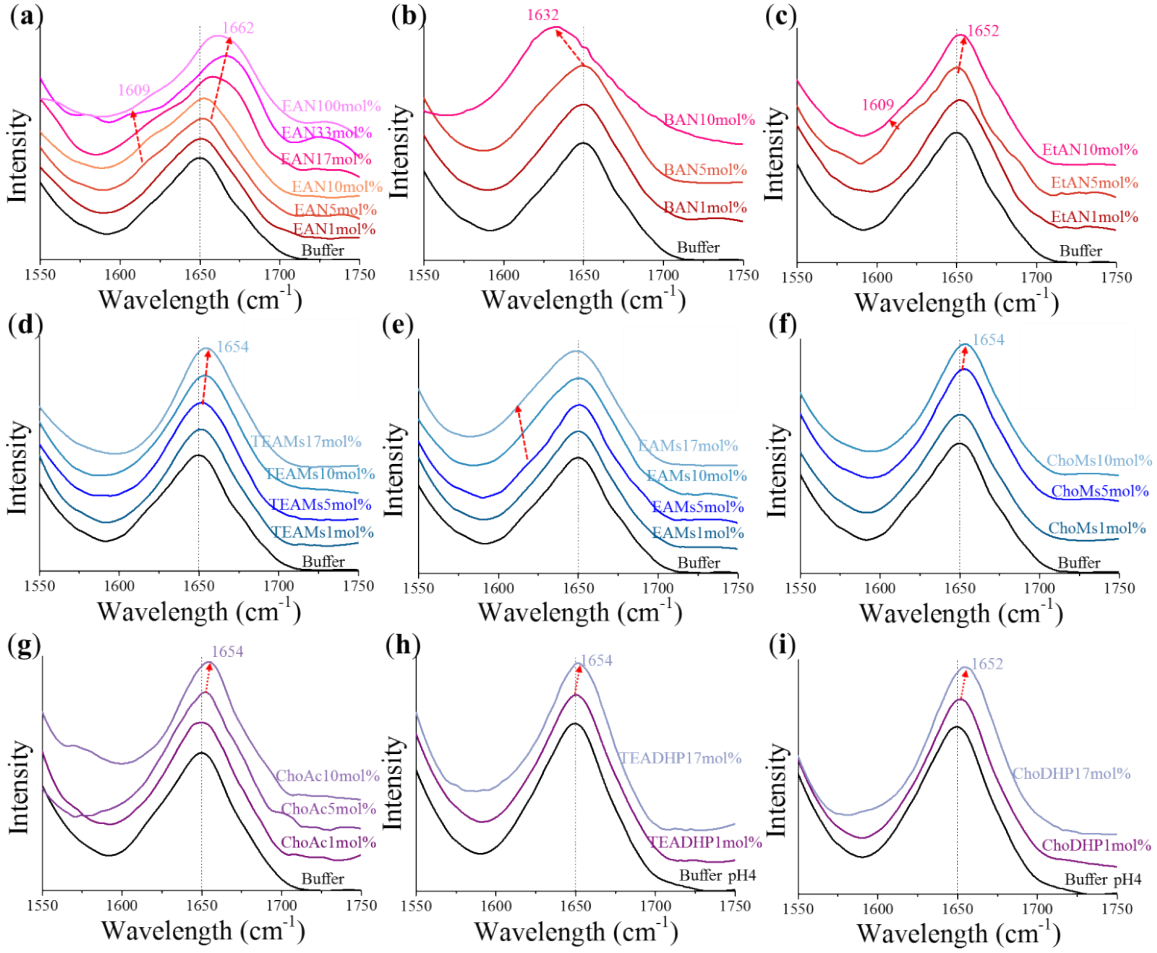

Figure 2. FTIR spectra of lysozyme in aqueous solutions of a) EAN, b) BAN, c) EtAN, d) TEAMs, e) EAMs, f) ChoMs, g) ChoAc, h) TEADHP and (i) ChoDHP. The control sample of lysozyme in a buffer at the same pH (pH 8 or pH 4), is included for comparison in each series. The red arrows refer to the shift of the amide I band, and the numbers indicate the wavenumber of the shifted peak position. The intensities are offset to enable easier comparison of the different samples.

In general, all the spectra of lysozyme with ILs present are symmetric at 1 mol% and 5 mol%, demonstrating that the α-helix content was maintained[30]. However, there were noticeable changes with 10 mol% IL present for nearly all the ILs, and this was attributed to the loss of helical structure, along with possible aggregate formation (shoulders around 1680 cm^{-1} [30, 45]). In the two additional nitrate-based ILs, namely BAN and EtAN (Figures 2b and 2c), it is evident that the amide I band has a distinguishable shift with 10 mol% IL present. The amide I band in 10 mol% EtAN had a slight redshift and narrower peak, which is similar to what was seen in 10 mol% EAN. In contrast, a significant blueshift of lysozyme in 10 mol% BAN was observed,

suggesting a growing contribution of β-turn arrangements[30]. The amide I band of lysozyme in TEAMs, EAMs, ChoMs and ChoAc-water mixtures are shown in Figures 2d, 2e, 2f and 2g, respectively. These showed similar changes as a function of IL concentration for TEAMs, ChoMs and ChoAc, with the amide I band having a slight redshift at high IL concentrations, i.e. 10 and 17 mol%. These redshifts suggest the loss of helical structure, which was also observed in EAN and EtAN. However, while the peak for EAMs was broadened at 10 and 17 mol%, there was no evident peak shift (Figure 2e).

Figures 2h and 2i show that the amide I band of lysozyme had a negligible change in 1 mol% TEADHP and ChoDHP compared to lysozyme in the pH 4 buffer. Similarly, there was little change to the amide I band in 17 mol% ChoDHP, which is in agreement with a previous study on ChoDHP[47]. However, lysozyme in 17 mol% TEADHP showed a marked redshift, indicating structural change had occurred.

Fluorescence spectroscopy was subsequently used to investigate the conformational changes of lysozyme in the IL-water mixtures. The spectra for all IL-lysozyme samples are provided in Figure S1 of the ESI and can be represented by the maximum intensity of the fluorescence (I_{max}), and the shift in wavelength at the maxima (λ_{max}). Such changes are attributed to a polarity change of Tryptophan (Trp) residues in the protein globule[12, 48]. Lysozyme contains six helices, including A (5–15), B (25–36), C (80–83), D (88–101), E (109–115) and F (120–124), and a β-sheet and loops domain (41-79). Figure 3a shows the position of the six Trp residues in lysozyme, with four Trp residues in the α-helix regions and two Trp in the loops. As well, two of the Trp residues in the helix region are close to the active site, which includes residues Glu35 and Asp52 and are in the cleft of the lysozyme structure.

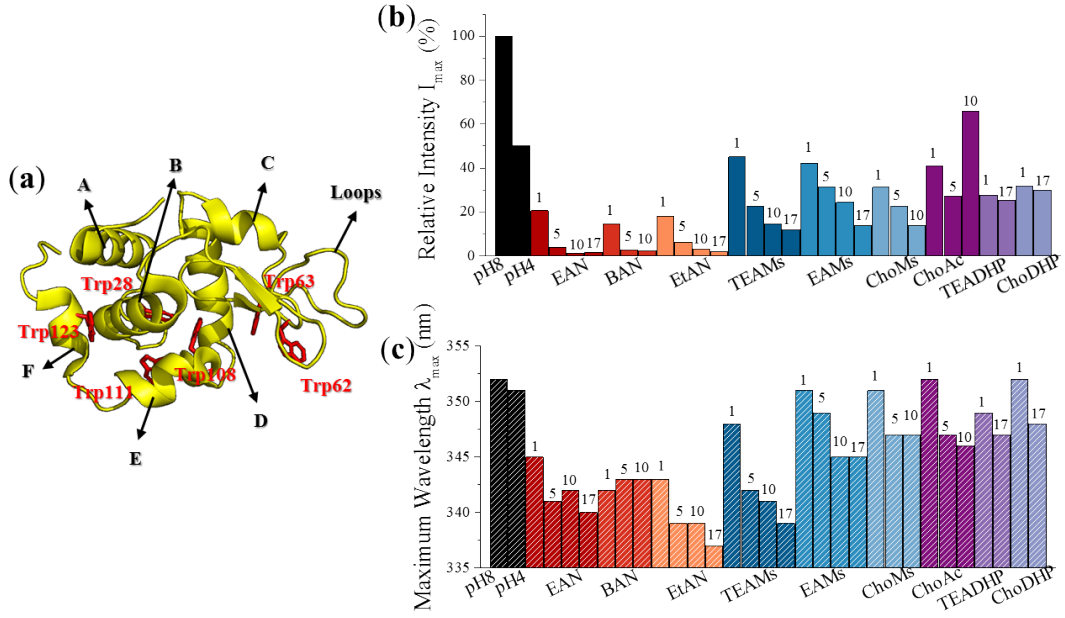

Figure 3. a) Location of Tryptophan (Trp) residues in Lysozyme, with the helical structures A-F and β-sheet and loop regions identified. Fluorescence spectra parameters of lysozyme in buffers at pH 8 and 4, and in IL-water mixtures for b) Maximum fluorescence intensity (I_{max}), and c) maximum wavelength (λ_{max}). The numbers in b) and c) are the mol% of the IL present.

Figures 3b and 3c show the relative I_{max} and λ_{max} of lysozyme fluorescence in the IL-water mixtures, and in the pH 8 and pH 4 buffers for comparison. For EAN, BAN and EtAN, the relative I_{max} was less than 20% of the pH 8 buffer, even with only 1 mol% of IL present (Figure 3b), and the three ILs all had a similar I_{max} at the same concentrations. The I_{max} decreased with increasing IL content, and was very low when the nitrate IL concentrations were 5 mol% or higher. In addition, the λ_{max} in these three ILs had a considerable shift to less than ~345 nm for all three concentrations, from 353 nm for the pH 8 buffer (Figures 3c). These decreases in I_{max} and redshifts in λ_{max} indicate that these nitrate-based ILs may alter the environment of the Trp residues of lysozyme through substantial conformational changes and interactions. It has been reported that the nitrate also quenched most of the fluorescence of tyrosinase, suggesting that the nitrate anion is possibly a quencher of Trp fluorescence[12].

Regarding the three mesylate-based ILs of TEAMs, EAMs and ChoMs, they all had I_{max} decrease as a function of IL concentration (Figure 3b). The relative I_{max} of these ILs was maintained at around 40%, 30% and 15% compared to the pH 8 buffer at 1, 5 and 10 mol%, respectively. Notably, their I_{max} was at least two times higher than the three nitrate-based ILs at

the same IL content. The λ_{max} of the three mesylate-based ILs had only a slight redshift (~5 nm) at 1 mol%, and a more significant redshift at higher IL concentrations (Figures 3c), particularly for TEAMs. For ChoAc, the relative I_{max} was similar to the mesylate based ILs for 1 and 5 mol% IL present, though it showed a significant increase at 10 mol% ChoAc (Figure 3b). However, we note that an increase in I_{max} does not always indicate enzyme stabilization[12, 18], and this increase may be related to the slight change observed for the secondary structure, based on its amide I region (Figure 2f).

Lysozyme retained ~60% of the intensity at both concentrations (i.e., 1 and 17 mol%) of TEADHP and ChoDHP, relative to the I_{max} in the pH 4 buffer. The λ_{max} experienced a slight redshift of less than 5 nm (Figure 3b), which suggests that the Trp residues may be relatively stable with these two ILs present. This is consistent with the FTIR spectra for lysozyme in these ILs (Figures 3h and 3i).

It is evident that the Trp fluorescence spectra of lysozyme are more sensitive than FTIR to changes in the ILs. This may be because the solvent exposure influences the strength and number of hydrogen bonds from the solvent to the lysozyme peptide groups. The anion of the ILs was observed to dominate the trends in the fluorescence intensity of lysozyme, with the degree of structural change from the IL anion following nitrate > mesylate > acetate and dihydrogen phosphate.

3.2. SAXS study of lysozyme - Structural analysis of lysozyme in solution

SAXS studies were performed to obtain information about the size and shape of lysozyme with the ILs present. Figure 4 shows the SAXS patterns of lysozyme in each IL-water mixture, with the radius of gyration (R_g) as a function of IL concentration provided in the inset. It should be noted that when 10 mol% of BAN was present there was a loss of intensity of lysozyme scattering for q above ~ 0.4 $Å^{-1}$ (Figure 4b), which was attributed to an artifact caused by the BAN nanostructure peak at ~0.7 $Å^{-1}$ [49]. For comparison, the SAXS patterns and R_g of lysozyme in standard buffers between pH 4 and 8 are provided in Figure S2. The uncertainties in the SAXS scattering are included in Figure S2, and are representative for the IL data. The R_g of lysozyme was ~14.3 at pH 7-8, which is consistent with the previous literature[50]. At pH 6 the R_g was 15.5 Å, with the slight increase attributed to this being the optimal pH of lysozyme[51]. The R_g decreased to 13.5 Å in the pH 4 buffer. It is reported that the radius of gyration (R_g) determined by SAXS is typically larger than that calculated from the atomic structure, owing

to the hydration layer[52]. Thus, to avoid breaking the hydration shell of lysozyme by ILs, the IL concentrations used in this study were below the hydration level for the protein [53].

Interestingly, for the nitrate and mesylate-based ILs, the R_g values of lysozyme increased with 1 mol% IL present, relative to R_g in the buffer, and then decreased with increasing IL content (Figure 4a-e), apart from ChoMs. After this decrease with increasing IL concentration the R_g values for lysozyme in the 17 mol% IL-water mixtures were still slightly higher than in the buffer. This suggests that the addition of these ILs results in the expansion of the lysozyme structure compared to that in the native state, with the greatest increase with 1 mol% of these ILs present. The SAXS patterns of lysozyme in the IL solutions of ChoMs, ChoAc, TEADHP and ChoDHP showed no obvious trends for their R_g values, and the values were between 15.5 and 16.5 Å, which was larger than the buffers at pH 8 and pH 4 (Table S1). This implies that the lysozyme structure is likely to expand in all IL solutions, or at least those containing between 1 to 17 mol% IL. The size increase of lysozyme as a more stretched state in the presence of salts (e.g., urea and guanidinium chloride) was reported previously[54-55], which is consistent with the increase seen for ILs. Previously, fluorescence correlation spectroscopy and molecular dynamics simulations have shown a reduction in size (hydrodynamic radius) of lysozyme in the IL 1-methyl-3-pentylimidazolium bromide[56]. In that study, it was observed that increasing the IL concentration from ~0.3 to ~2 mol% led to a decrease of the protein radius, which was attributed to the displacement of the water solvation layer by ILs, particularly by the cation. However, this was for an imidazolium-based cation, which is expected to have stronger interactions than the cations in this study.

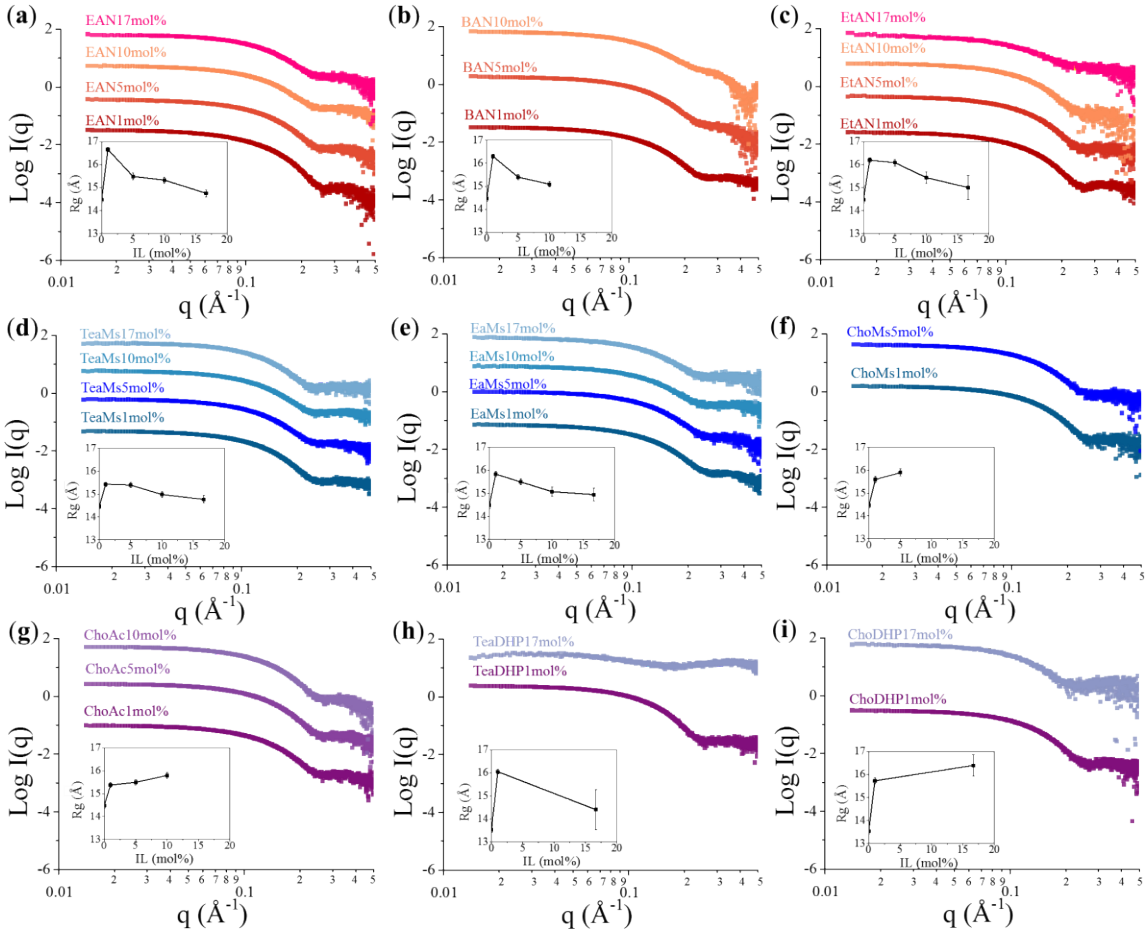

Figure 4. SAXS patterns of lysozyme in a) EAN, b) BAN, c) EtAN, d) TEAMs, e) EAMs, f) ChoMs, g) ChoAc, h) TEADHP and i) ChoDHP-water mixtures. The inset shows the radius of gyration, R_g, of lysozyme as a function of IL concentration, (based on Guinier plots provided in Figure S3). The offset was applied to readily enable visual comparison between the samples.

Furthermore, we investigated a selection of the IL-water mixtures at pH 6 to compare to the data collected at pH 8, and the SAXS patterns and R_g values are provided in Figure S4. There was negligible difference between the SAXS patterns or R_g values at the two pH values, which indicates small pH changes of IL-water mixtures are not critical in comparison with the IL type and concentration.

Figure S3 shows the Guinier plots, and these were linear for the region used to obtain R_g. It should be noted that the first twelve data points in the q range between 0.006 to 0.015 $Å^{-1}$ show very high variability (large error bars as indicated in Figure S3). These were probably affected by instrumental background noise close to the beamstop, and hence these data were not used for any subsequent analysis.

The shape classification of the data (Figure 4) and the Guinier region indicates the protein is monomeric and little aggregation was present. In Figure S5, we observed a single P(r) peak for most ILs, which is consistent with monodisperse spheres. This resulting P(r) vs r profile further reveals that lysozyme forms a relatively consistent and monomeric structure with a R_g of 13-15 Å in all ILs (Table S2). In addition, small tails are observed in the P(r) function in the presence of most of these ILs, with a maximum particle dimension (D_{max}) of ~60 Å (Table S2). This further demonstrates that lysozyme had a slightly extended conformation in IL solutions. There were subpeaks in the P(r) function for 10 mol% BAN and 17 mol% EtAN and small shoulders for 10 mol% TEAMs, 5 mol% EAMs, 17 mol% EAMs and 17 mol% ChoDHP. These may be due to conformational changes in specific areas of lysozyme, which were also observed in the spectroscopic study, or may be artifacts due to the data transformation into real space. No meaningful P(r) could be obtained from the data for 17 mol% TEADHP.

In general, the R_g and P(r) peak did not significantly change on the addition of these ILs, suggesting that lysozyme is unlikely to be significantly unfolded at high concentration of ILs. In addition, the Kratky plots (Figure S6) exhibit decreased intensity of the bell-shaped curve with increasing IL concentrations, demonstrating the well-folded structure of lysozyme is maintained, though its flexibility increased somewhat in the presence of the ILs. Such flexibility is likely related to the extended structure in the ILs.

The SAXS data for the lysozyme with 1 and 5 mol% ILs was further analyzed. These IL concentrations were selected due to their monodispersed P(r) profiles (Figure S5). The lysozyme crystallographic structure (PDB: 1dpw, crystallized in 100 mM buffer) was initially fitted to the data using normal-mode analysis, followed by fitting the SAXS data with SREFLEX[34]. The modeling in SREFLEX uses the PDB structure as a starting point, then probes large conformational rearrangements and smaller localized movements to identify possible conformational changes to improve the fit to the experimental data. Figure 5 shows the initial lysozyme models (highlighted as yellow) with initial discrepancies χ^2 values when fitting the 1dpw PDB structure to the SAXS data, and the adjusted models after the SREFLEX adjustment. The statistical discrepancies χ^2 values are provided with ~1.00 being the optimally adjusted models. Some large χ^2 values could be due to the inherent limitation of SAXS-based refinement approaches for smaller conformational changes.

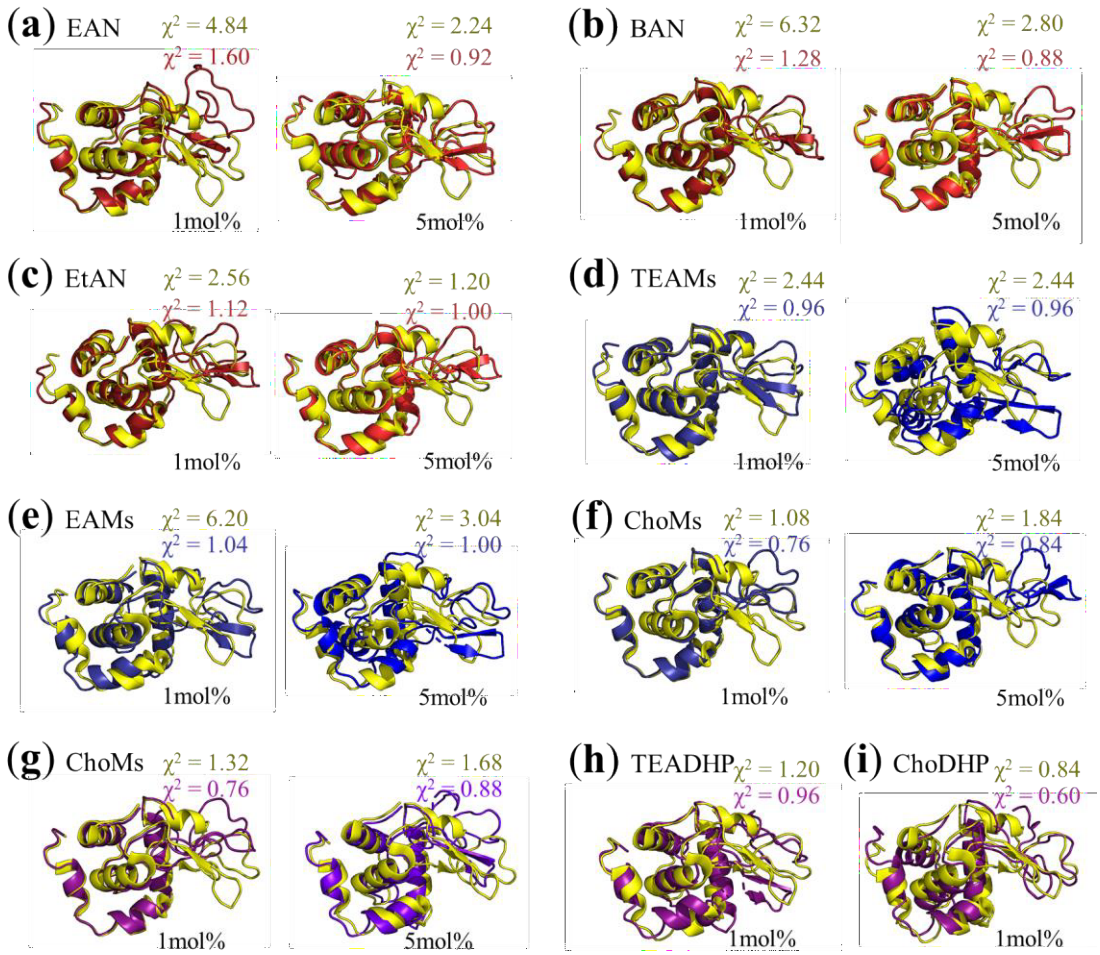

Figure 5. SREFLEX models of lysozyme in buffer (yellow) and IL-water mixtures at 1 mol% and 5 mol%: (a) EAN, (b) BAN, (c) EtAN, (d) TEAMs, (e) EAMs, (f) ChoMs, (g) ChoMs, (h) TEADHP and (i) ChoDHP. SREFLEX models were fitted based on corresponding SAXS patterns (Figure 4) and the crystal structure of lysozyme (PDB:1dpw, Figure S7). The discrepancies χ^2 values of the initial model and the refined model were provided for each IL. based on discrepancies χ^2 value from the modelling.

In general, the adjusted models show little conformational changes in the helical structures with either 1 or 5 mol% ILs present. However, the lysozyme models in all the ILs, particularly 5 mol% of TEAMs or EAMs, experienced a slight rotation and orientation in the helical structures, and an orientation in the β-sheet structures. As α-helix and β-sheets are supported by hydrogen-bonded strands, these regions on the protein surface may undergo slight transitions due to IL exposure[30]. Such orientation in the secondary structures may result in the changes seen for the Trp fluorescence. In addition, all the adjusted models were more stretched than the crystallographic model, particularly in the loop regions. This is because these loops are

intrinsically flexible and can adopt many different conformations[30]. In the three nitrate-based ILs at 1 mol% (Figures 5a-c), a more extended loop region was seen, whereas this region was slightly more compacted with 5 mol% of the nitrate ILs present. The flexibility in the loops was also observed for lysozyme with ~2 mol% of 1-methyl-3-pentylimidazolium bromide by fluorescence correlation spectroscopy and molecular dynamic simulation[57]. Additionally, the χ^2 values for these 1 mol% nitrate-based ILs were over 1.1, which are larger than what is normally considered a reasonable value. This suggests that in addition to the major changes noted above, the nitrate ions are also causing a few minor conformation changes which the SREFLEX refinement process did not identify.

The lysozyme conformation in ChoMs and ChoAc showed relatively small changes (Figures 5f and g), which suggests that they may be effective solvents for maintaining the structure. This is reflected by only slight changes in the FTIR spectra and Trp fluorescence (Figures 2f, 2g and 3), and are in agreement with a previous study[58]. For TEADHP and ChoDHP (Figures 5h and i), the α-helix and β-sheet regions of lysozyme are shifted relative to the PDB 1dpw structure. These slight conformational changes in the secondary structure, along with the extended conformational changes in the loop regions, indicate that lysozyme is a stable protein with relatively flexible regions, agreeing with the previous concept of lysozyme as a "hard" protein[59].

The models obtained using SREFLEX for lysozyme in 10 and 17 mol% EAN, TEAMs and EAMs are provided in Figure S8. These show significant changes in the structures of lysozyme, indicating lysozyme may be unfolded or denatured. Thus, high concentration of these ILs may be unfavorable for lysozyme. It has been recognized that ILs may lower the protein–water interfacial tension and thus interact with the protein surface[58, 60]. It should be noted that the high salt concentrations (over 10 mol% in our study) contain ion pairs with electrostatic interactions with the protein[61]. Moreover, the high concentration of ILs could provide additional IL–protein interactions, which are dependent on the specific IL.

3.3. X-ray crystallographic analysis of lysozyme

We used X-ray crystallography for lysozyme in 1 mol% EAN to evaluate in detail the conformation of lysozyme in the presence of an IL. Images of the lysozyme crystals are provided in Figure S9, and the crystallography statistics in Table S3. Crystal sizes varied between 10-50 μm in the longest length and 5-25 μm in the shorter direction. It is worth noting

that, to the best of our knowledge, this is the first study using a batch method and IL-water mixtures (in the absence of other nucleating agents) for protein crystallization. With a resolution of 1.2 Å, we were able to explore the specific conformational changes of lysozyme, and the specific interactions between EAN and lysozyme.

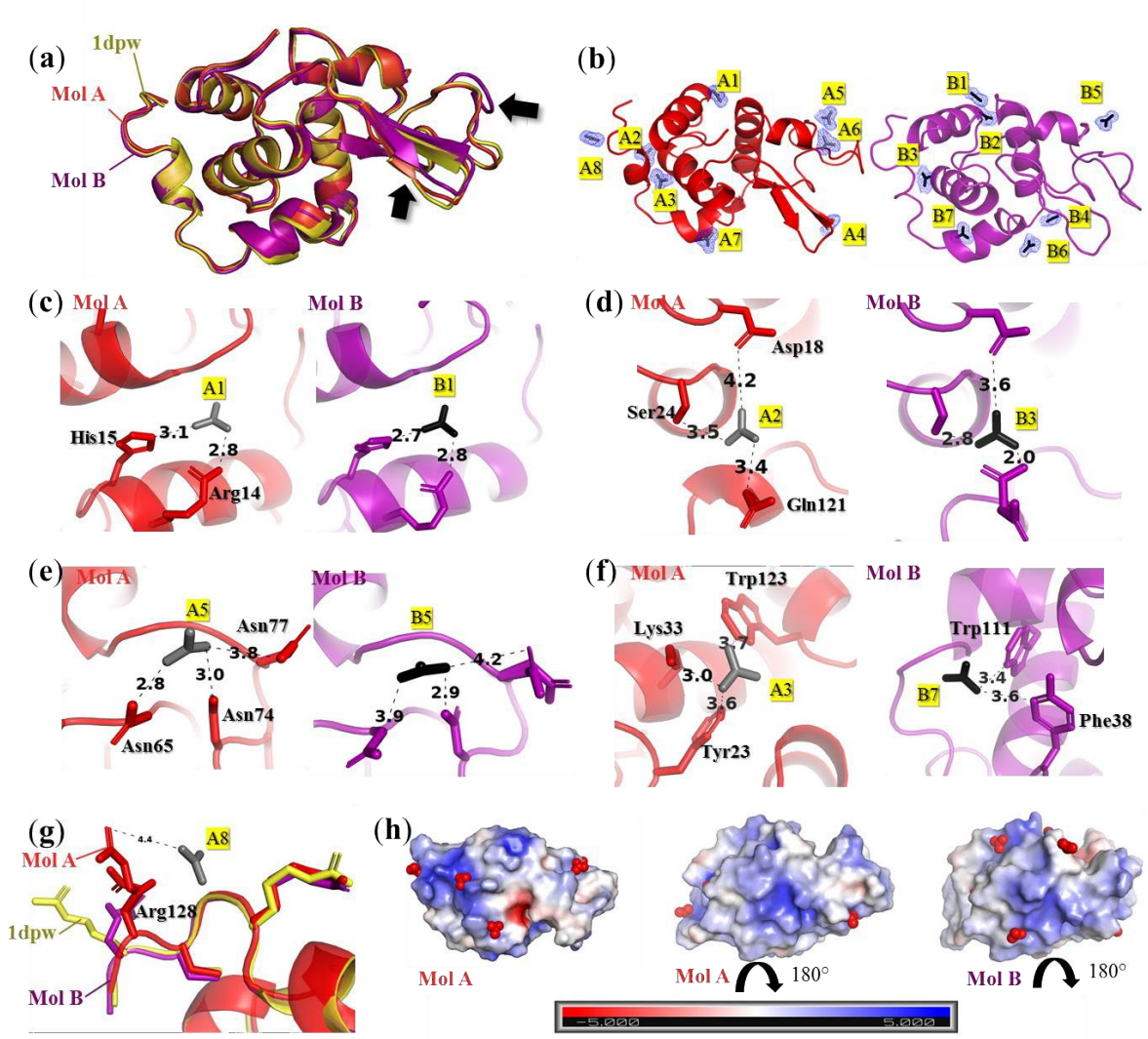

Figure 6. Crystal structural analysis of lysozyme in 1 mol% EAN-water mixture. The structure was solved to 1.2 Å resolution. a) Cartoon representation of the two molecules of lysozyme in a unit cell including molecule A (Mol A, red) and molecule B, (Mol B, purple) superposed with the published crystal model, PDB 1dpw (yellow), the black arrows indicate the changes in β-sheet and loops regions; b) Cartoon representation of Mol A and B with associated simulated annealing Fo-Fc omit maps of the labeled nitrate ions (A1-A7 in Mol A and B1-B7 in Mol B) from EAN contoured in blue; Specific nitrate ions binding interactions with the molecules are shown in c) A1 and B1, d) A2 and B3, e) A4 and B4; f) Specific interaction between nitrate

ions with Trp residues; g) Specific interaction between nitrate ions A7 with Arg128 residue; h) Surface charge representation of the lysozyme structure with nitrate ions present, where the red and blue colors correspond to negative and positive electrostatic potentials, respectively.

The overall structure in 1 mol% of EAN was analyzed to a unit cell, space group $P12_11$ with two molecules (molecule A (Mol A) and molecule B (Mol B) in Figure 6a), which is consistent with literature values for the unit cell of lysozyme[62]. Compared with the published lysozyme structure (PDB ID 1dpw), the overall structure in 1 mol% of EAN showed little change (RMSD value of 0.389 for Mol A and 0.489 for Mol B). However, the two molecules showed noticeable changes in the β-sheet and loops regions, with slight expansions (residues 41-79 in Mol B, Figure 6a). In addition, there was a slight loss of α-helix structure in residues 109-110 in Mol A, and residues 120-124 in Mol B. These changes agree with the SREFLEX model for the SAXS data of lysozyme in 1 mol% of EAN (Figure 6a), but to a lesser extent. Considering the proteins are more dynamic in solutions, the lysozyme conformation in solutions observed by SAXS is more flexible. While crystal packing forces may confine the flexibility of the lysozyme structure during crystallization in the IL solution, inducing less subdomain-level conformational changes than what is seen in solution. However, changes in the loop region (residues 41-79) were evident both in solution and crystallized lysozyme in 1 mol% EAN, indicating that these are the areas affected by the nitrate ions.

Eight nitrate ions from EAN were identified in the crystal structures for Mol A and seven for Mol B as directly interacting with lysozyme. These were labeled A1-A7 and B1-B7 for the lysozyme molecules of Mol A and B, respectively, and are shown in Figure 6b. However, these nitrate interactions did not appear to contribute significantly to the conformational changes within the secondary structure of lysozyme but more on the peripheral solvent exposed areas of the protein. Importantly, all nitrate ions had hydrogen bonding with water molecules (Figure S10) and tend to interact with the lysozyme surface. This is owing to the displacement of the hydration layer by the IL[56]. Four of these nitrates were located in anion-binding pockets that seemed to be non-specific in both molecules, while three of the nitrates had specific binding (hydrogen bonds with distances around 4 Å) in the α-helix and loop and turn regions (Figures 6c-e). These nitrate ions interacted with the same amino acids in both molecules. For example, both A1 and B1 nitrates interacted with Arg14 and His15, while both A2 and B3 nitrates interacted with Asp18, Ser 24 and Gln121. Both A4 and B4 nitrate ions interacted with three

Asn residues (65, 74 and 77). The nitrate ions seemed to have no preference to certain amino acids as they hydrogen bonded to different amino acids.

Interestingly, we observed an interaction between the nitrate ion and Trp residues. Two different binding sites were identified in Figure 6f, with nitrate A3 bound to both Trp123 and Tyr23 in Mol A, while nitrate B7 interacted with Trp111 and Phe38 in Mol B. The binding of the nitrate ions in this area may account for the fluorescence changes detected in the fluorescence spectroscopy. The chromophore residues were blocked, leading to the decrease in fluorescence intensity which was observed for lysozyme in EAN (Figure 2). It was noted that the nitrate A3 and B7 bound to two water molecules on the protein surface, indicating that these interactions affect the protein solvation layer, although the hydration shell was observed to be retained.

Specific interactions between nitrate A4 and B4 and the loop region (residue 41-79) were observed. Along with nitrates A5 and B5, these bonds may induce the overall conformational changes in the loop regions. In addition, it is noted that the interaction between nitrate A7 and Arg 128 in the N-terminal is an ionic bond, resulting in conformational changes of the amino acid in Mol A (Figure 6g). Similar ionic bonding was also observed in the previous study using sodium nitrate as the nucleating agent for lysozyme[63]. However, it seems that such ionic bonding is non-specific since the majority of 11 Arg residues in lysozyme did not bond with the nitrate. The regions favored by the nitrate ions are shown in Figure 6h. The nitrate ions are generally bound with the positively charged areas rather than specific amino acids. In contrast, the ethylammonium cation was not found in the electron density map of lysozyme. This is consistent with our findings, and previous reports, that the anions of ILs dominate their interactions with proteins[63]. Here we demonstrated that the anion of EAN directly interacts with the surface residues of lysozyme, whereas the cation did not, and the main interactions likely involved charged surface areas.

4. Conclusion

We have investigated the conformational changes of a model protein, lysozyme, in nine IL-water mixtures both low and high concentrations. In contrast to previous studies where lysozyme was shown to be unfolded with high concentrations of ILs[14-17, 56], we found lysozyme predominantly retained its native structure with some small changes in all the IL solutions in this study. FTIR and fluorescence spectroscopic studies demonstrated that the amide I region experienced a significant change with concentrations of 10 mol% ILs or greater, and that nitrate ions have a large effect on the Tryptophan residues. SAXS data and modelling revealed that lysozyme in the presence of 1 and 5 mol% ILs may have subtle changes in the helix structures, and slightly expanded β-sheets and loop regions. This flexibility at 1 and 5 mol% is similar to those previously observed in aqueous IL solutions[56], however, higher IL concentrations generally led to the structure becoming more compact, with a noticeable change in the β-sheet structures. X-ray crystallography of lysozyme crystals grown in 1 mol% ethylammonium nitrate (EAN) identified that EAN affected the loops region of lysozyme (residue 41-79), which led to a noticeable increase in the overall volume. Specific interactions between the nitrate ions of EAN and the protein surface were identified, *viz*., hydrogen bonds and an ionic bonding network with the protein surface residues. The binding of nitrate anions to Tryptophan residues was attributed to causing the change in fluorescence of lysozyme in the presence of nitrate ILs. The positively charged areas on the surface of lysozyme were identified as favored sites for the nitrate ions. These findings show for the first time the interaction between an IL and lysozyme at an atomic level. This study proves IL-water mixtures are viable solvents for maintaining protein conformations, and has significant implications for manufacturing and health related uses of proteins.

Acknowledgements

This research was undertaken in part on the SAXS/WAXS beamline and MX2 beamline at the Australian Synchrotron, Melbourne, Australia.

Data availability

The authors declare that all relevant data are included in the paper and its Supplementary Information. The SAXS raw data are available at the following Figshare repository (10.25439/rmt.12705056).

CRediT authorship contribution statement

Qi Han: Conceptualization, Methodology, Investigation, Formal analysis, Writing - original draft, Writing - review & editing, Visualization. **Kate M. Smith:** Methodology, Investigation, Resources, Validation, Writing - review & editing. **Connie Darmanin:** Methodology, Resources, Validation, Writing - review & editing. **Timothy M. Ryan:** Methodology, Resources, Validation, Writing - review & editing. **Calum J. Drummond1:** Investigation, Resources, Writing - review & editing, Supervision, Project administration. **Tamar Greaves:** Conceptualization, Methodology, Investigation, Formal analysis, Writing - review & editing, Supervision, Project administration.

References

1. Scharnagl, C.; Reif, M.; Friedrich, J., Stability of proteins: Temperature, pressure and the role of the solvent. *Biochimica et Biophysica Acta (BBA) - Proteins and Proteomics* **2005,** *1749* (2), 187-213.

2. Balcão, V. M.; Vila, M. M. D. C., Structural and functional stabilization of protein entities: state-of-the-art. *Adv Drug Deliv Rev* **2015,** *93*, 25-41.

3. Iyer, P. V.; Ananthanarayan, L., Enzyme stability and stabilization—Aqueous and non-aqueous environment. *Process Biochem* **2008,** *43* (10), 1019-1032.

4. Jessop, P. G., Searching for green solvents. *Green Chem Lett Rev* **2011,** *13* (6), 1391-1398.

5. van Rantwijk, F.; Sheldon, R. A., Biocatalysis in ionic liquids. *Chem Rev* **2007,** *107* (6), 2757-2785.

6. Zhao, H., Protein stabilization and enzyme activation in ionic liquids: specific ion effects. *J Chem Technol Biot* **2016,** *91* (1), 25-50.

7. Welton, T., Room-temperature ionic liquids. Solvents for synthesis and catalysis. *Chem Rev* **1999,** *99* (8), 2071-2083.

8. Greaves, T. L.; Drummond, C. J., Protic ionic liquids: Properties and applications. *Chem Rev* **2008,** *108* (1), 206-237.

9. MacFarlane, D. R.; Kar, M.; Pringle, J. M., *Fundamentals of Ionic Liquids: From Chemistry to Applications*. John Wiley & Sons: 2017.

10. Yoshizawa, M.; Xu, W.; Angell, C. A., Ionic Liquids by Proton Transfer: Vapor Pressure, Conductivity, and the Relevance of ΔpKa from Aqueous Solutions. *J Am Chem Soc* **2003,** *125* (50), 15411-15419.

11. Kohno, Y.; Ohno, H., Ionic liquid/water mixtures: from hostility to conciliation. *Chem Commun* **2012,** *48* (57), 7119-7130.

12. Lai, J. Q.; Li, Z.; Lu, Y. H.; Yang, Z., Specific ion effects of ionic liquids on enzyme activity and stability. *Green Chem* **2011,** *13* (7), 1860-1868.

13. Takekiyo, T.; Ishikawa, Y.; Yoshimura, Y., Cryopreservation of proteins using ionic liquids: a case study of cytochrome c. *J Phys Chem B* **2017,** *121* (32), 7614-7620.

14. Byrne, N.; Wang, L. M.; Belieres, J. P.; Angell, C. A., Reversible folding-unfolding, aggregation protection, and multi-year stabilization, in high concentration protein solutions, using ionic liquids. *Chem Commun* **2007,** (26), 2714-2716.

15. Yoshimura, Y.; Takekiyo, T.; Mori, T., Structural study of lysozyme in two ionic liquids at cryogenic temperature. *Chem Phys Lett* **2016,** *664*, 44-49.

16. Strassburg, S.; Bermudez, H.; Hoagland, D., Lysozyme Solubility and Conformation in Neat Ionic Liquids and Their Mixtures with Water. *Biomacromolecules* **2016,** *17* (6), 2233-2239.

17. Wijaya, E. C.; Separovic, F.; Drummond, C. J.; Greaves, T. L., Stability and activity of lysozyme in stoichiometric and non-stoichiometric protic ionic liquid (PIL)-water systems. *J Chem Phys* **2018,** *148* (19), 193838.

18. Han, Q.; Wang, X.; Byrne, N., Understanding the Influence of Key Ionic Liquid Properties on the Hydrolytic Activity of Thermomyces lanuginosus Lipase. *Chemcatchem* **2016,** *8* (8), 1551-1556.

19. Han, Q.; Wang, X.; Byrne, N., A Simple Approach to Achieve Self-Buffering Protic Ionic Liquid-Water Mixtures. *ChemistrySelect* **2017,** *2* (15), 4294-4299.

20. Greaves, T. L.; Drummond, C. J., Protic Ionic Liquids: Evolving Structure-Property Relationships and Expanding Applications. *Chem Rev* **2015,** *115* (20), 11379-11448.

21. Fujita, K.; MacFarlane, D. R.; Forsyth, M.; Yoshizawa-Fujita, M.; Murata, K.; Nakamura, N.; Ohno, H., Solubility and stability of cytochrome c in hydrated ionic liquids: effect of oxo acid residues and kosmotropicity. *Biomacromolecules* **2007,** *8* (7), 2080-2086.

22. Arunkumar, R.; Drummond, C. J.; Greaves, T. L., FTIR Spectroscopic Study of the Secondary Structure of Globular Proteins in Aqueous Protic Ionic Liquids. *Frontiers in Chemistry* **2019,** *7*, 74.

23. Kong, J.; Yu, S., Fourier transform infrared spectroscopic analysis of protein secondary structures. *Acta Biochim Biophys Sin* **2007,** *39* (8), 549-559.

24. Rambo, R. P.; Tainer, J. A., Super-resolution in solution X-ray scattering and its applications to structural systems biology. *Annu Rev Biophys* **2013,** *42*, 415-441.

25. Bui-Le, L.; Clarke, C. J.; Bröhl, A.; Brogan, A. P.; Arpino, J. A.; Polizzi, K. M.; Hallett, J. P., Revealing the complexity of ionic liquid–protein interactions through a multi-technique investigation. *Comm Chem* **2020,** *3* (1), 1-9.

26. Reddy, R. R.; Shanmugam, G.; Madhan, B.; Kumar, B. P., Selective binding and dynamics of imidazole alkyl sulfate ionic liquids with human serum albumin and collagen–a detailed NMR investigation. *Phys Chem Chem Phys* **2018,** *20* (14), 9256-9268.

27. Chen, X.; Ji, Y.; Wang, J., Improvement on the crystallization of lysozyme in the

presence of hydrophilic ionic liquid. *Analyst* **2010,** *135* (9), 2241-2248.

28. Mertens, H. D.; Svergun, D. I., Structural characterization of proteins and complexes using small-angle X-ray solution scattering. *J Struct Biol* **2010,** *172* (1), 128-141.

29. Trewhella, J.; Duff, A. P.; Durand, D.; Gabel, F.; Guss, J. M.; Hendrickson, W. A.; Hura, G. L.; Jacques, D. A.; Kirby, N. M.; Kwan, A. H., 2017 publication guidelines for structural modelling of small-angle scattering data from biomolecules in solution: an update. *Acta Crystallogr D* **2017,** *73* (9), 710-728.

30. Demirdöven, N.; Cheatum, C. M.; Chung, H. S.; Khalil, M.; Knoester, J.; Tokmakoff, A., Two-dimensional infrared spectroscopy of antiparallel β-sheet secondary structure. *J Am Chem Soc* **2004,** *126* (25), 7981-7990.

31. Belieres, J.-P.; Angell, C. A., Protic Ionic Liquids: Preparation, Characterization, and Proton Free Energy Level Representation†. *J Phys Chem B* **2007,** *111* (18), 4926-4937.

32. Han, Q.; Wang, X.; Bynre, N., Utilizing water activity as a simple measure to understand hydrophobicity in ionic liquids. *Front Chem* **2019,** *7*.

33. Wijaya, E. C.; Separovic, F.; Drummond, C. J.; Greaves, T. L., Activity and conformation of lysozyme in molecular solvents, protic ionic liquids (PILs) and salt–water systems. *Phys Chem Chem Phys* **2016,** *18* (37), 25926-25936.

34. Panjkovich, A.; Svergun, D. I., Deciphering conformational transitions of proteins by small angle X-ray scattering and normal mode analysis. *Phys Chem Chem Phys* **2016,** *18* (8), 5707-5719.

35. Ryan, T. M.; Trewhella, J.; Murphy, J. M.; Keown, J. R.; Casey, L.; Pearce, F. G.; Goldstone, D. C.; Chen, K.; Luo, Z.; Kobe, B.; McDevitt, C. A.; Watkin, S. A.; Hawley, A. M.; Mudie, S. T.; Samardzic Boban, V.; Kirby, N., An optimized SEC-SAXS system enabling high X-ray dose for rapid SAXS assessment with correlated UV measurements for biomolecular structure analysis. *J Appl Crystallogr* **2018,** *51* (1), 97-111.

36. Jeffries, C. M.; Graewert, M. A.; Blanchet, C. E.; Langley, D. B.; Whitten, A. E.; Svergun, D. I., Preparing monodisperse macromolecular samples for successful biological small-angle X-ray and neutron-scattering experiments. *Nat Protoc* **2016,** *11* (11), 2122-2153.

37. Weiss, M. S.; Palm, G. J.; Hilgenfeld, R., Crystallization, structure solution and refinement of hen egg-white lysozyme at pH 8.0 in the presence of MPD. *Acta Crystallogr D* **2000,** *56* (8), 952-958.

38. Ritchie, A. W.; Webb, L. J., Optimizing electrostatic field calculations with the adaptive

Poisson–Boltzmann solver to predict electric fields at protein–protein interfaces II: explicit near-probe and hydrogen-bonding water molecules. *J Phys Chem B* **2014,** *118* (28), 7692-7702.

39. Aragao, D.; Aishima, J.; Cherukuvada, H.; Clarken, R.; Clift, M.; Cowieson, N. P.; Ericsson, D. J.; Gee, C. L.; Macedo, S.; Mudie, N., MX2: a high-flux undulator microfocus beamline serving both the chemical and macromolecular crystallography communities at the Australian Synchrotron. *Journal of Synchrotron Radiat* **2018,** *25* (3), 885-891.

40. Kabsch, W., Xds. *Acta Crystallogr D* **2010,** *66* (2), 125-132.

41. Winn, M. D.; Ballard, C. C.; Cowtan, K. D.; Dodson, E. J.; Emsley, P.; Evans, P. R.; Keegan, R. M.; Krissinel, E. B.; Leslie, A. G.; McCoy, A., Overview of the CCP4 suite and current developments. *Acta Crystallogr D* **2011,** *67* (4), 235-242.

42. McCoy, A. J.; Grosse-Kunstleve, R. W.; Adams, P. D.; Winn, M. D.; Storoni, L. C.; Read, R. J., Phaser crystallographic software. *J Appl Crystallogr* **2007,** *40* (4), 658-674.

43. Casañal, A.; Lohkamp, B.; Emsley, P., Current developments in Coot for macromolecular model building of Electron Cryo-microscopy and Crystallographic Data. *Protein Sci* **2020,** *29* (4), 1069-1078.

44. Liebschner, D.; Afonine, P. V.; Baker, M. L.; Bunkoczi, G.; Chen, V. B.; Croll, T. I.; Hintze, B.; Hung, L.-W.; Jain, S.; McCoy, A. J.; Moriarty, N. W.; Oeffner, R. D.; Poon, B. K.; Prisant, M. G.; Read, R. J.; Richardson, J. S.; Richardson, D. C.; Sammito, M. D.; Sobolev, O. V.; Stockwell, D. H.; Terwilliger, T. C.; Urzhumtsev, A. G.; Videau, L. L.; Williams, C. J.; Adams, P. D., Macromolecular structure determination using X-rays, neutrons and electrons: recent developments in Phenix. *Acta Crystallogr D* **2019,** *75* (10), 861-877.

45. Pechkova, E.; Innocenzi, P.; Malfatti, L.; Kidchob, T.; Gaspa, L.; Nicolini, C., Thermal stability of lysozyme Langmuir− Schaefer films by FTIR spectroscopy. *Langmuir* **2007,** *23* (3), 1147-1151.

46. Sassi, P.; Giugliarelli, A.; Paolantoni, M.; Morresi, A.; Onori, G., Unfolding and aggregation of lysozyme: A thermodynamic and kinetic study by FTIR spectroscopy. *J Biophys Chem* **2011,** *158* (1), 46-53.

47. Weaver, K. D.; Vrikkis, R. M.; Van Vorst, M. P.; Trullinger, J.; Vijayaraghavan, R.; Foureau, D. M.; McKillop, I. H.; MacFarlane, D. R.; Krueger, J. K.; Elliott, G. D., Structure and function of proteins in hydrated choline dihydrogen phosphate ionic liquid. *Phys Chem Chem Phys* **2012,** *14* (2), 790-801.

48. Sternberg, M. J., *Protein Structure Prediction: A Practical Approach: A Practical*

Approach. Oxford University Press, USA: 1996.

49. Greaves, T. L.; Kennedy, D. F.; Mudie, S. T.; Drummond, C. J., Diversity observed in the nanostructure of protic ionic liquids. *J Phys Chem B* **2010,** *114* (31), 10022-10031.

50. Huang, Y.-S.; Jeng, U.-S.; Shiu, Y.-J.; Lai, Y.-H.; Sun, Y.-S., Charge interaction and temperature effects on the solution structure of lysozyme as revealed by small-angle X-ray scattering. *J Appl Crystallogr* **2007,** *40* (s1), s165-s169.

51. Chang, K. Y.; Carr, C. W., Studies on the structure and function of lysozyme: I. The effect of pH and cation concentration on lysozyme activity. *J Biochimica et Biophysica Acta* **1971,** *229* (2), 496-503.

52. Svergun, D.; Richard, S.; Koch, M.; Sayers, Z.; Kuprin, S.; Zaccai, G., Protein hydration in solution: experimental observation by x-ray and neutron scattering. *Proc Natl Acad Sci* **1998,** *95* (5), 2267-2272.

53. Ohno, H.; Fujita, K.; Kohno, Y., Is seven the minimum number of water molecules per ion pair for assured biological activity in ionic liquid-water mixtures? *Phys Chem Chem Phys* **2015,** *17* (22), 14454-14460.

54. Chowdhury, R.; Mojumdar, S. S.; Chattoraj, S.; Bhattacharyya, K., Effect of ionic liquid on the native and denatured state of a protein covalently attached to a probe: solvation dynamics study. *J Chem Phys* **2012,** *137* (5), 055104.

55. Xia, Z.; Das, P.; Shakhnovich, E. I.; Zhou, R., Collapse of unfolded proteins in a mixture of denaturants. *J Am Chem Soc* **2012,** *134* (44), 18266-18274.

56. Ghosh, S.; Parui, S.; Jana, B.; Bhattacharyya, K., Ionic liquid induced dehydration and domain closure in lysozyme: FCS and MD simulation. *J Chem Phys* **2015,** *143* (12), 09B622_1.

57. Nandi, S.; Parui, S.; Halder, R.; Jana, B.; Bhattacharyya, K., Interaction of proteins with ionic liquid, alcohol and DMSO and in situ generation of gold nano-clusters in a cell. *J Biophys Rev* **2018,** *10* (3), 757-768.

58. Kowacz, M.; Mukhopadhyay, A.; Carvalho, A. L.; Esperança, J. M.; Romão, M. J.; Rebelo, L. P. N., Hofmeister effects of ionic liquids in protein crystallization: Direct and water-mediated interactions. *Crystengcomm* **2012,** *14* (15), 4912-4921.

59. Kubiak-Ossowska, K.; Mulheran, P. A., Mechanism of Hen Egg White Lysozyme Adsorption on a Charged Solid Surface. *Langmuir* **2010,** *26* (20), 15954-15965.

60. Zeindlhofer, V.; Schröder, C., Computational solvation analysis of biomolecules in aqueous ionic liquid mixtures. *Biophys Rev* **2018,** *10* (3), 825-840.

61. Zhang, Y.; Cremer, P. S., The inverse and direct Hofmeister series for lysozyme. *Proc Natl Acad Sci* **2009,** *106* (36), 15249-15253.

62. Garlitz, J. A.; Summers, C. A.; Flowers, R. A.; Borgstahl, G. E., Ethylammonium nitrate: a protein crystallization reagent. *Acta Crystallogr D* **1999,** *55* (12), 2037-2038.

63. Steinrauf, L., Structures of monoclinic lysozyme iodide at 1.6 Å and of triclinic lysozyme nitrate at 1.1 Å. *J Acta Crystallogr D* **1998,** *54* (5), 767-779.